Applied Physics Letters ARTICLE pubs.aip.org/aip/apl

Tunneling-enhanced interface recombination and current loss curves in kesterite solar cells

Cite as: Appl. Phys. Lett. **123**, 242102 (2023); doi: 10.1063/5.0175082
Submitted: 5 September 2023 · Accepted: 30 November 2023 ·
Published Online: 12 December 2023

Jüri Krustok,[a] Kristi Timmo, Marit Kauk-Kuusik, and Maarja Grossberg-Kuusk

AFFILIATIONS

Department of Materials and Environmental Technology, Tallinn University of Technology, Ehitajate tee 5, 19086 Tallinn, Estonia

[a]Author to whom correspondence should be addressed: Juri.Krustok@taltech.ee

ABSTRACT

An approach to developing durable, light-weight, flexible, and semi-transparent solar cells is through the utilization of Cu_2ZnSnS_4 (CZTS) monograin powder. However, CZTS cells are currently far from their theoretically predicted efficiency. One reason for this is tunneling-enhanced interface recombination, which leads to a decrease in V_{OC} and FF under higher forward bias conditions. We calculated the current loss curves J_R–V of three different CZTS monograin layer solar cells for this report by subtracting the dark J–V curve from the light curve and adding a short circuit current density J_{SC}. By quantum tunneling of holes through a bell-shaped potential barrier with additional recombination at the interface between CdS and CZTS, the shape of the current loss curve was examined. We showed that using the derivative dJ_R/dV of the measured curves allows us to simplify our analysis. The maximum position of this curve is proportional to the effective barrier height, and the intensity and the full width at half maximum give information about the width. At lower temperatures, the effective barrier height increases according to our theoretical model. We demonstrated that the properties of CZTS solar cells may be significantly enhanced by eliminating current loss at higher bias voltages.

Photovoltaic (PV) electricity generation has been developing quickly over the past 10 years, and this trend is expected to continue in the future, making PV's sustainable development more and more crucial. The utilization of abundant materials in the creation of a PV device is particularly alluring when considering sustainable development. The kesterite-structured Cu_2ZnSnS_4 (CZTS) and $Cu_2ZnSnSe_4$ (CZTSe), formed by combining abundant metals like copper, zinc, and tin with chalcogen elements such as sulfur and selenium, serve as an alternative absorber layer in thin film photovoltaics. Thin film PV research in CZTS is gaining interest because of its strong absorption coefficient ($\alpha \approx 10^4\,cm^{-1}$) over a significant portion of the AM1.5 spectrum. The Shockley–Queisser limit states that its wide bandgap range of 1.0–1.5 eV (by tuning S/Se ratio) provides a theoretical maximum efficiency between 20% and 30%.[1]

However, to be competitive with other thin film PV technologies, CZTS devices must prioritize improved efficiency and reduced manufacturing costs. Kesterite solar cells now have a certified total area efficiency of 13.8%, whereas CdTe, chalcopyrite, and perovskite cells have efficiencies of above 22%.[2] It is well acknowledged that open-circuit voltage V_{OC} continues to be the biggest issue with the kesterite solar cell technology.[3,4] One of the major factors limiting the performance of kesterite solar cells is the presence of defects and recombination centers in the absorber layer and at the interfaces with other layers. The typical device structure of a kesterite solar cell consists of a glass substrate coated with a transparent conductive oxide (TCO) layer, such as indium tin oxide (ITO) or zinc oxide (ZnO), followed by a thin n-type buffer layer, such as cadmium sulfide (CdS) or zinc sulfide (ZnS), a p-type kesterite absorber layer, and a metallic back contact, such as molybdenum (Mo) or nickel (Ni). The buffer layer plays an important role in forming a heterojunction with the absorber layer and enhancing the collection of photogenerated charge carriers. However, it can also introduce interface defects and recombination centers that can degrade the device performance. The most commonly used buffer layer for kesterite solar cells is CdS, which has been successfully applied also in chalcopyrite solar cells. CdS has a bandgap of 2.4 eV and forms a type-II heterojunction with CZTS, which creates a favorable band alignment for charge carrier separation and transport. However, CdS also has some drawbacks, such as its toxicity, its lattice mismatch with CZTS, its potential formation of secondary phases with Cu or Zn at high temperatures, and its high conduction band offset with CZTS, which can create a barrier for electron transport and increase interface recombination.[5] Numerous investigations have demonstrated that one of the primary recombination channels in kesterite solar cells is the tunneling-enhanced interface recombination.[6–10] The

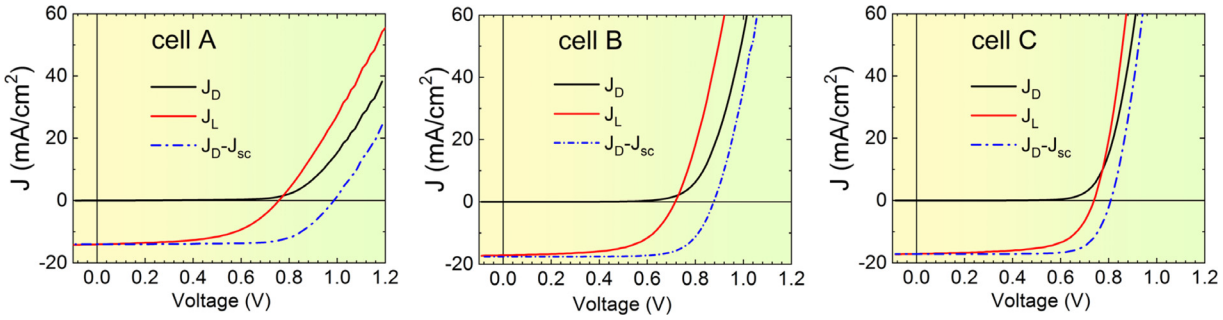

FIG. 1. Dark (J_D) and light (J_L) J–V curves, and J_{SC} shifted dark curves (J_D–J_{SC}) for all cells.

band bending works as a barrier for holes tunneling from CZTS into interface states of the heterojunction, where various traps may be involved in recombination. A similar, but lower, barrier is also formed for electrons due to the conduction band offset between CZTS and CdS layers. However, as it was already demonstrated for $Cu(In,Ga)Se_2$ (CIGS) solar cells, the critical barrier is related to holes.[11] In these solar cells, the $Cu(In,Ga)_3Se_5$ phase [ordered vacancy compound (OVC)] as a surface layer creates an additional barrier for holes and significantly improves the properties of the heterojunction between CIGS and CdS.[12] The i-ZnO layer's ability to effectively block holes was also found to have the same effect in perovskite solar cells.[13] Thus, in order to lower interface recombination in all types of solar cells, the potential barrier for holes is crucial. More and more holes can tunnel into the interface region and recombine with electrons as the height of this barrier decreases with forward bias. Therefore, at higher values of forward bias, we start to see current loss. In this report, we will introduce an alternative method for analyzing tunneling-enhanced interface recombination and demonstrate how this phenomenon leads to increase in current loss in CZTS/CdS monograin layer solar cells.

The CZTS absorber of a monograin layer solar cell is made up of tiny (diameter ~50 μm) single crystals that are placed in an epoxy layer and function as individual solar cells. More details about preparation of monograin layer solar cells can be found in previous papers.[6,14–16] These CZTS solar cells often show a crossover between the illuminated and dark J–V characteristics.[17] This phenomenon is frequently explained by voltage-dependent photogeneration; however, there are other scenarios that could result in a general current loss of solar cells. One of them is related to tunneling-enhanced interface recombination at higher forward bias. The loss of photogenerated carriers leads to a decrease in the open circuit voltage V_{OC} and fill factor FF of solar cells.

In general, the current density–voltage relation of a CZTS-based solar cell can be described by Chan and Phang[18]

$$J = J_0\left\{\exp\left[\frac{q(V+JR_S)}{nkT}\right]-1\right\}+\frac{V+JR_S}{R_{sh}}-J_L, \quad (1)$$

where $J_0 = J_{00}\exp\left(\frac{-\Phi_B}{nkT}\right)$. Φ_B is the activation energy of the saturation current J_0, q is the electron charge, n is the ideality factor, R_s is the series resistance, R_{sh} is the shunt resistance, V is the terminal voltage, kT is the thermal energy, and J_L is the photocurrent. Eq. (1) states that the J_L-shifted dark and light curves must have the same shape, with n values ranging from 1 to 2, assuming that R_s and R_{sh} remain relatively constant. In fact, the light J–V curve has a different shape compared to the dark curve, and the gap becomes more pronounced as the forward bias voltage V increases, see Fig. 1. Therefore, the light curves' ideality factors often exhibit values of $n > 2$. The temperature dependence of the diode ideality factor n typically provides valuable knowledge regarding potential recombination mechanisms in solar cells. It was demonstrated that the temperature dependence of the ideality factor in the context of tunneling-enhanced interface recombination is provided by Refs. 19–21

$$n = \frac{E_{00}}{\alpha kT}\coth\left(\frac{E_{00}}{kT}\right), \quad (2)$$

where the E_{00} is a characteristic tunneling energy, and $\alpha = [\omega_p/\varepsilon_p]/[\omega_p/\varepsilon_p + \omega_n/\varepsilon_n]$, where ω_p, ω_n, and ε_p, ε_n are the space charge region widths and dielectric constants of the absorber and the buffer, respectively. Our earlier research demonstrates that Eq. (2) can often provide an excellent fit to n vs T curves, and that the tunneling energy E_{00} is typically in the region of 50 meV.[6,10] Additionally, the V_{OC} vs T and $n\ln(J_0)$ vs T^{-1} curves both yield activation energies lower than the bandgap energy E_g, which is proof that interface recombination is one of the most powerful in CZTS solar cells.[19,22] It is evident that tunneling-enhanced interface recombination causes a current loss in solar cells. At higher voltages, this loss is particularly noticeable because the band bending and consequently the potential barrier for carriers are lower. For further analysis, we chose three different CZTS monograin layer solar cells, the parameters of which are listed in Table I. We deliberately chose solar cells with

TABLE I. Parameters for three different CZTS solar cells under study. Last values with an asterisk (*) are hypothetical values without interface recombination losses calculated from J_D–J_{SC} curves, see Fig. 1.

Cell	A	B	C
V_{OC} (mV)	757	716	739
J_{SC} (mA/cm^2)	14.0	17.1	17.1
FF (%)	55.4	61.7	64.4
Efficiency (%)	5.9	7.5	8.1
Ideality factor n	3.01	2.89	2.25
V_{OC}^* (mV)	992	877	775
FF^* (%)	67.5	73.3	76.5
Efficiency* (%)	9.4	11.3	10.1

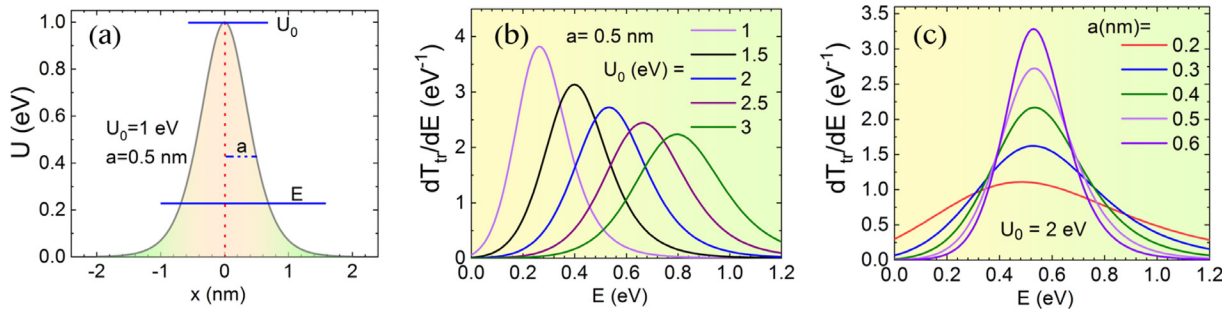

FIG. 2. (a) The shape of a potential barrier for carriers in CZTS solar cells; (b) the shape of the dT_{tr}/dE curve as a function of barrier height U_0; and (c) the shape of the dT_{tr}/dE curve as a function of barrier halfwidth a.

radically different parameters. The composition of CZTS monograins was $Cu_{1.93}Zn_{1.06}Sn_{1.02}S_4$, $Cu_{1.92}Zn_{1.07}Sn_{1.01}S_4$, and $Cu_{1.91}Zn_{1.09}Sn_{1.01}S_4$ for cells A, B, and C, respectively. Monograins for A and C cells were grown in KI salt, while RbI salt was used for cell B. All cells had a surface area of 0.045 cm^2 and were measured under standard test conditions (AM 1.5, 100 mW cm^{-2}) using a Newport Oriel Class A 91195 A solar simulator. Figure 1 provides J–V curves for all cells, and all obtained parameters are given in Table I.

It is evident that in the absence of a current loss, the V_{OC}, FF, and efficiency of all cells increase, see Table I. The current loss curves (J_R) for all cells are calculated as $J_R = J_L - J_D + J_{SC}$ and are presented in Fig. 3(a). The current loss curve's shape is typical for the tunneling process, in which low voltage and a high barrier height prohibit charge carriers from crossing the barrier and initiate an interfacial recombination. The current loss curve shows saturation at higher voltages, indicating that practically all holes can pass through the barrier. The actual shape of this potential barrier is not known, but most likely, it has a bell-like or triangular shape. Schrödinger equations must be solved in order to determine the transmission coefficient (T_{tr}) of a potential barrier, and in many instances, this can only be done numerically. Therefore, we selected a barrier shape with an analytical solution $U(x) = U_0/\cosh(x/a)^2$, where $(U_0,\ a > 0)$, a is related to the width of the barrier, and U_0 is the height of the barrier, see Fig. 2(a).[23] The transmission T_{tr} of this barrier is given by

$$T_{tr} = \frac{\sinh^2\left(\pi\sqrt{2\epsilon}\right)}{\sinh^2\left(\pi\sqrt{2\epsilon}\right) + \cosh\left(\frac{\pi}{2}\right)\sqrt{8u_0 - 1}}, \tag{3}$$

where $u_0 = ma^2U_0/\hbar^2$ and $\epsilon = ma^2E/\hbar^2$, m is a hole effective mass, and E is the energy of charge carriers. T_{tr} has values between 0 and 1. Figure 2 demonstrates the dT_{tr}/dE curves as a function of barrier height U_0 (b) and barrier halfwidth a (c).

The analysis of the current loss curves (J_R) for several CZTS solar cells has revealed that the T_{tr} function predominantly governs the shape of these curves. However, there is often a linear portion at lower voltages, which is attributed to changes in R_{sh} for both dark and light J–V curves. Interestingly, we did not observe significant differences between the serial resistance R_s of dark and light curves. Therefore, we excluded the role of R_s change from further analysis.

It is known that the barrier halfwidth a decreases as $a \sim c_a\sqrt{V_0 - V}$, where constant c_a includes also a role of carrier concentration, i.e., light intensity, and that the barrier height U_0 lowers linearly with increasing voltage $U_0 \sim q(V_0 - V)$.[24] Here, V_0 is related to the barrier height. We can define new variables $\epsilon^* = c_1 * a^2kT$ and $u_0^* = c_2 * a^2(V_0 - V)$, where c_1 and c_2 are constants, and kT is a

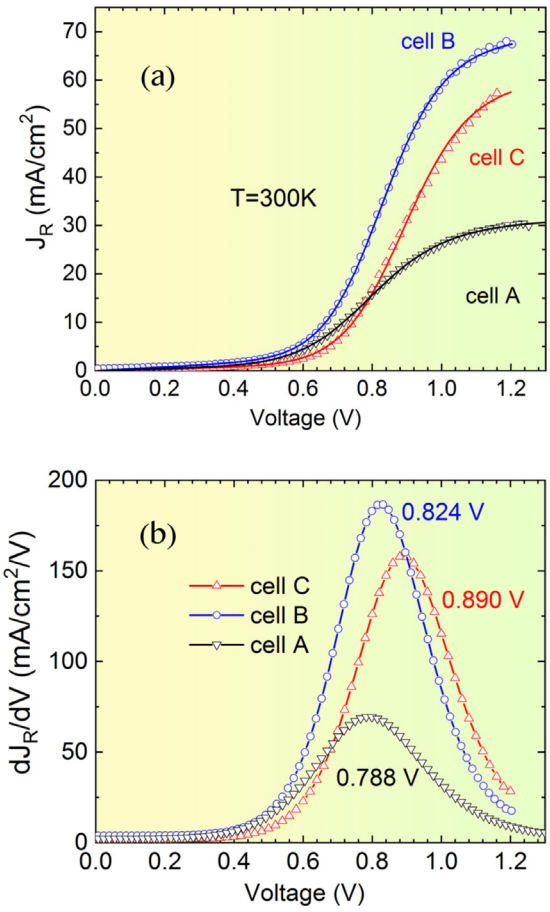

FIG. 3. (a) Room temperature current loss (J_R) curves for three different cells (dots), and the fitting results (lines) using Eq. (4) and (b) for three different solar cells, the first derivative of the J_R is plotted against the forward bias. Derivative maximum positions are listed.

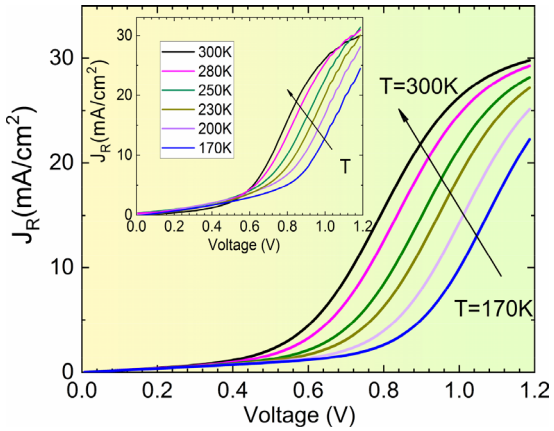

FIG. 4. Calculated temperature dependence of J_R for cell A. Inset shows experimentally measured temperature dependence of current loss curves for cell A.

thermal energy of holes. Both these variables include also the barrier width a. As a result, the shape of the J_R curve can be expressed as

$$J_R(V) = J_{R0} * T_{tr}\left(\epsilon^*, u_0^*, T, V\right) + c_3 * V, \tag{4}$$

where c_3 is related to shunt resistance differences between dark and light curves. J_{R0} defines the maximum current loss through this recombination process and is related also to J_{SC}. Figure 3(a) shows a result of fitting with Eq. (4) for three different CZTS solar cells. All solar cells show an ideal fit with Eq. (4). Although Eq. (4) provides a perfect fit to current loss curves that have been measured experimentally, it contains a substantial number of fitting parameters. This means that it is highly likely that different combinations of these parameters will give very close fitting results. In addition, it will be quite challenging to give a physical meaning to all fitting parameters. Therefore, we chose the derivative dJ_R/dV of the measured curves to simplify our analysis, and the results are shown in Fig. 3(b). The position of the derivative maximum V_m is directly related to the effective potential barrier height U_0–E and does not depend on J_{SC}, while the intensity of the dJ_R/dV curve is linked to the extent of this barrier and to J_{SC}, see Fig. 2. In order to get information about barrier width without the role of the generated current J_{SC}, we can use the full width at half maximum (FWHM) of derivative curves. According to Fig. 2(c), the FWHM is inversely proportional to the barrier width. According to our analysis, cells A, B, and C's FWHM values were 381, 316, and 332 mV, respectively. We can observe that cell A, which has a moderate efficiency, has the derivative maximum at the lowest voltage and lowest barrier width, while cell C, which has a larger efficiency, also has the highest effective barrier height. The cell A's high FWHM value and low V_m indicate that the recombination loss begins to affect the J–V curve at lower voltages, which causes a decrease in FF when compared to other cells.

The transmission of holes through the potential barrier also depends on temperature because of the thermal energy of the holes $E = kT$. We took previously obtained fitting parameters for cell A and calculated the temperature dependence of the J_R function by keeping all parameters constant and changing only the temperature in the range of 170–300 K. The results of these calculations are given in Fig. 4.

We also measured the temperature dependence of the same cell by inserting it into a cold finger of a closed-cycle He cryostat. The obtained J_R curves are presented as an inset in Fig. 4. It is clear that the theoretical model predicts the measured temperature dependence of the current loss curve J_R quite well. It is obvious that the position of the derivative maximum V_m also depends on temperature. Lower temperatures decrease the thermal energy of charge carriers and increase the effective barrier height U_0–E. As a result, the maximum of the dJ_R/dV curve shifts toward higher voltages. Indeed, the analysis of experimental J_R curves demonstrates an almost linear relationship between the maximum position of derivative V_m and temperature, see Fig. 5(b). At the same time, the FWHM of the derivative curves did not change much and has values around 400 mV. This fact proves that the width of the barrier is not significantly affected by temperature, but rather determined by the properties of the heterojunction. Figure 5(b) shows the temperature dependence of V_m with the linear fit. We see that the maximum barrier height (1.50 eV at T = 0 K) for this cell is very close to the bandgap energy E_g of CZTS.[10,25–27]

Our analysis indicates that the recombination at the CZTS/CdS interface might be effectively mitigated by introducing an additional layer with lower valence band edge on top of the CZTS absorber, similar to the OVC layer used in CIGS/CdS solar cells. The presence of this layer hinders the tunneling of holes, making it less likely for them to pass through the potential barrier and thus increasing the V_{OC} and FF of CZTS solar cells.

In conclusion, three different CZTS monograin solar cells' current loss curves were examined. To describe the shape of the current loss curve and its temperature dependence, a theoretical model of

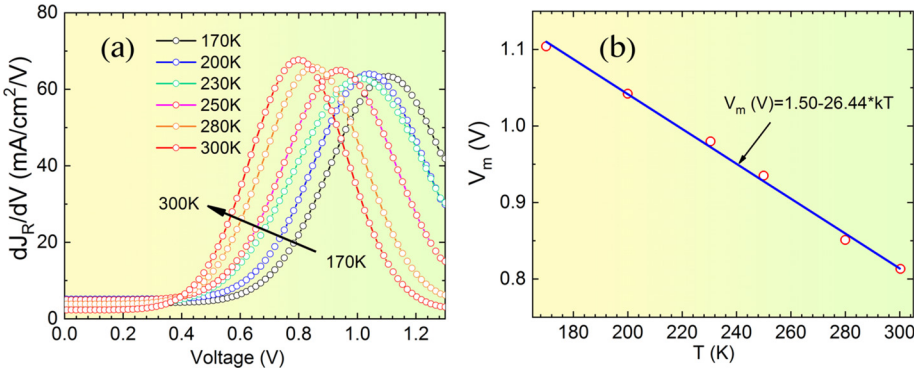

FIG. 5. (a) Temperature dependence of the dJ_R/dV function for the cell A and (b) temperature dependence of the derivative maximum V_m, linear fit is given as a line.

quantum tunneling of holes through a bell-shaped potential barrier was created. We also demonstrated that it is possible to obtain important details about potential barrier properties by using the derivative dJ_R/dV of the measured curves. We demonstrated that the properties of CZTS solar cells may be significantly enhanced by eliminating current loss at higher bias voltages.

This work was supported by the European Union's H2020 research and innovation program under Grant Agreement No. 952982 (Custom-Art project), and by the Estonian Research Council Grant No. PRG1023.

AUTHOR DECLARATIONS

Conflict of Interest

The authors have no conflicts to disclose.

Author Contributions

Jüri Krustok: Conceptualization (lead); Data curation (lead); Formal analysis (lead); Writing – original draft (lead); Writing – review & editing (lead). **Kristi Timmo:** Resources (equal); Writing – review & editing (supporting). **Marit Kauk-Kuusik:** Resources (equal); Writing – review & editing (supporting). **Maarja Grossberg-Kuusk:** Funding acquisition (lead); Writing – review & editing (supporting).

DATA AVAILABILITY

The data that support the findings of this study are available from the corresponding author upon reasonable request.

REFERENCES

[1]L. Sravani, S. Routray, M. Courel, and K. P. Pradhan, Sol. Energy **227**, 56 (2021).
[2]J. Zhou, X. Xu, H. Wu, J. Wang, L. Lou, K. Yin, Y. Gong, J. Shi, Y. Luo, D. Li, H. Xin, and Q. Meng, Nat. Energy **8**, 526 (2023).
[3]M. He, C. Yan, J. Li, M. P. Suryawanshi, J. Kim, M. A. Green, and X. Hao, Adv. Sci. **8**, 2004313 (2021).
[4]S. Giraldo, Z. Jehl, M. Placidi, V. Izquierdo-Roca, A. Pérez-Rodríguez, and E. Saucedo, Adv. Mater. **31**, 1806692 (2019).
[5]N. Naghavi, D. Abou-Ras, N. Allsop, N. Barreau, S. Bücheler, A. Ennaoui, C.-H. Fischer, C. Guillen, D. Hariskos, J. Herrero, R. Klenk, K. Kushiya, D. Lincot, R. Menner, T. Nakada, C. Platzer-Björkman, S. Spiering, A. N. Tiwari, and T. Törndahl, Prog. Photovoltaics **18**, 411 (2010).
[6]M. Kauk-Kuusik, K. Timmo, K. Muska, M. Pilvet, J. Krustok, M. Danilson, V. Mikli, R. Josepson, and M. Grossberg-Kuusk, J. Phys.: Energy **4**, 024007 (2022).
[7]M. Courel, J. A. Andrade-Arvizu, and O. Vigil-Galán, Mater. Res. Express **3**, 095501 (2016).
[8]M. Kauk-Kuusik, K. Timmo, K. Muska, M. Pilvet, J. Krustok, R. Josepson, G. Brammertz, B. Vermang, M. Danilson, and M. Grossberg, ACS Appl. Energy Mater. **4**, 12374 (2021).
[9]F. Liu, C. Yan, J. Huang, K. Sun, F. Zhou, J. A. Stride, M. A. Green, and X. Hao, Adv. Energy Mater. **6**, 1600706 (2016).
[10]K. Timmo, M. Altosaar, M. Pilvet, V. Mikli, M. Grossberg, M. Danilson, T. Raadik, R. Josepson, J. Krustok, and M. Kauk-Kuusik, J. Mater. Chem. A **7**, 24281 (2019).
[11]Y. Zhao, S. Yuan, Q. Chang, Z. Zhou, D. Kou, W. Zhou, Y. Qi, and S. Wu, Adv. Funct. Mater. **31**, 2007928 (2021).
[12]T. Ogihara, A. Sadono, T. Nishimura, K. Nakada, and A. Yamada, Jpn. J. Appl. Phys., Part 1 **56**, 062301 (2017).
[13]W. Hadouchi, J. Rousset, D. Tondelier, B. Geffroy, and Y. Bonnassieux, RSC Adv. **6**, 67715 (2016).
[14]J. Li, K. Sun, X. Yuan, J. Huang, M. A. Green, and X. Hao, npj Flex. Electron. **7**, 16 (2023).
[15]D. Meissner, K. Ernits, S. Gahr, L. Kapitan, M. Vetter, C. Glatz, and R. Syed, Sol. Energy Mater. Sol. Cells **252**, 112160 (2023).
[16]M. Kauk-Kuusik, K. Timmo, M. Pilvet, K. Muska, M. Danilson, J. Krustok, R. Josepson, V. Mikli, and M. Grossberg-Kuusk, J. Mater. Chem. A **11**, 23640 (2023).
[17]M. Buffière, G. Brammertz, S. Oueslati, H. E. Anzeery, J. Bekaert, K. Ben Messaoud, C. Köble, S. Khelifi, M. Meuris, and J. Poortmans, J. Phys. D: Appl. Phys. **47**, 175101 (2014).
[18]D. S. H. Chan and J. C. H. Phang, IEEE Trans. Electron Devices **34**, 286 (1987).
[19]U. Rau, A. Jasenek, H. Schock, F. Engelhardt, and T. Meyer, Thin Solid Films **361-362**, 298 (2000).
[20]U. Rau, Appl. Phys. Lett. **74**, 111 (1999).
[21]V. Nadenau, U. Rau, A. Jasenek, and H. W. Schock, J. Appl. Phys. **87**, 584 (2000).
[22]M. Danilson, E. Kask, N. Pokharel, M. Grossberg, M. Kauk-Kuusik, T. Varema, and J. Krustok, Thin Solid Films **582**, 162 (2015).
[23]F. M. Fernández, Am. J. Phys. **79**, 752 (2011).
[24]S. S. Li, *Semiconductor Physical Electronics* (Springer, 2006).
[25]V. V. Rakitin, P. E. Varushkin, H. Xin, and G. F. Novikov, EPJ Photovoltaics **10**, 6 (2019).
[26]G. Altamura and J. Vidal, Chem. Mater. **28**, 3540 (2016).
[27]P. K. Sarswat and M. L. Free, Physica B **407**, 108 (2012).